Supporting Information

Tin Assisted Fully Exposed Platinum Clusters Stabilized on Defect-Rich Graphene for Dehydrogenation Reaction

Jiayun Zhang,[1, 2 #] *Yuchen Deng,*[3#] *Xiangbin Cai,*[4 #] *Yunlei Chen,*[5, 6 #] *Mi Peng,*[3] *Zhimin Jia,* [1, 2] *Zheng Jiang,*[7] *Pengju Ren,*[5, 6] *Siyu Yao,*[3] *Jinglin Xie,*[3] *Dequan Xiao,*[8] *Xiaodong Wen,* [5, 6] *Ning Wang,* [4 *] *Hongyang Liu,* [1, 2 *] *and Ding Ma,* [3*]

[1] Shenyang National Laboratory for Materials Science, Institute of Metal Research, Chinese Academy of Sciences, Shenyang 110016, P. R. China.

[2] School of Materials Science and Engineering, University of Science and Technology of China, Hefei 230026, P. R. China.

[3] Beijing National Laboratory for Molecular Sciences, College of Chemistry and Molecular Engineering and College of Engineering, and BIC-ESAT, Peking University, Beijing 100871, P. R. China.

[4] Department of Physics and Center for Quantum Materials, Hong Kong University of Science and Technology, Clear Water Bay, Kowloon, HongKong SAR, P. R. China.

[5] State Key Laboratory of Coal Conversion, Institute Coal Chemistry, Chinese Academy of Sciences, Taiyuan 030001, P. R. China.

[6] University of Chinese Academy of Science, No. 19A Yuanquan Road, Beijing 100049, P. R. China.

[7] Shanghai Institute of Applied Physics, Chinese Academy of Sciences, Shanghai 201204, P. R. China.

[8] Center for Integrative Materials Discovery, Department of Chemistry and Chemical Engineering, University of New Haven, 300 Boston Post Road, West Haven, Connecticut 06516, United States.

[*]Corresponding Author. Email: liuhy@imr.ac.cn; phwang@ust.hk; dma@pku.edu.cn

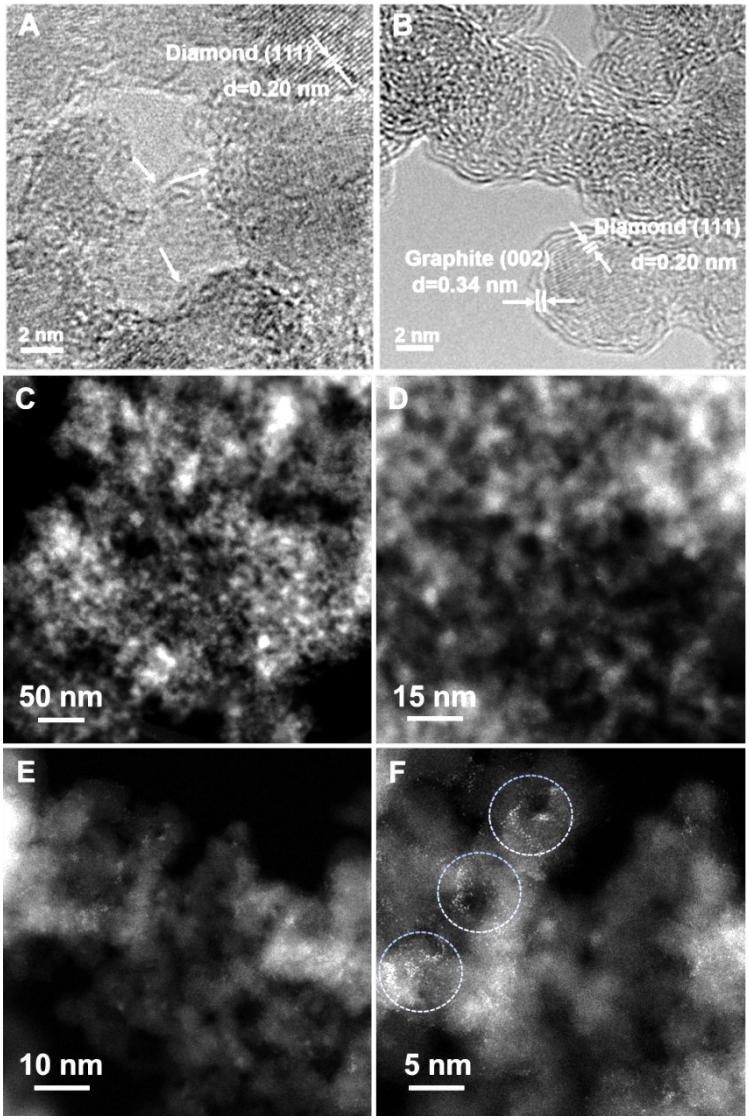

fig. S1. HRTEM images of **A**) the pristine ND and **B**) the ND@G. **C-F)** HAADF-STEM image of the Sn/ND@G catalyst with 0.5 wt% Sn.

The HRTEM images of the pristine ND and the ND@G hybrid support are displayed in **fig S1A-B**. The amorphous carbon can be seen on ND surface (as labeled by the white arrows). After calcination at 1100 ^{o}C, this amorphous carbon can be transferred into 2-3 layers of graphene nanoshell, while particular morphology with a size of 4-8 nm of the original ND phase is well maintained.[1] For the ND@G hybrid support, these defect-rich graphitic outer layer are curved and structurally reinforced by the ND core.[2] The HAADF-STEM image of the Sn/ND@G catalyst displayed in **fig S1C-F** indicated that the Sn can be homogenously dispersed on the ND@G support as marked in **fig S1F.**

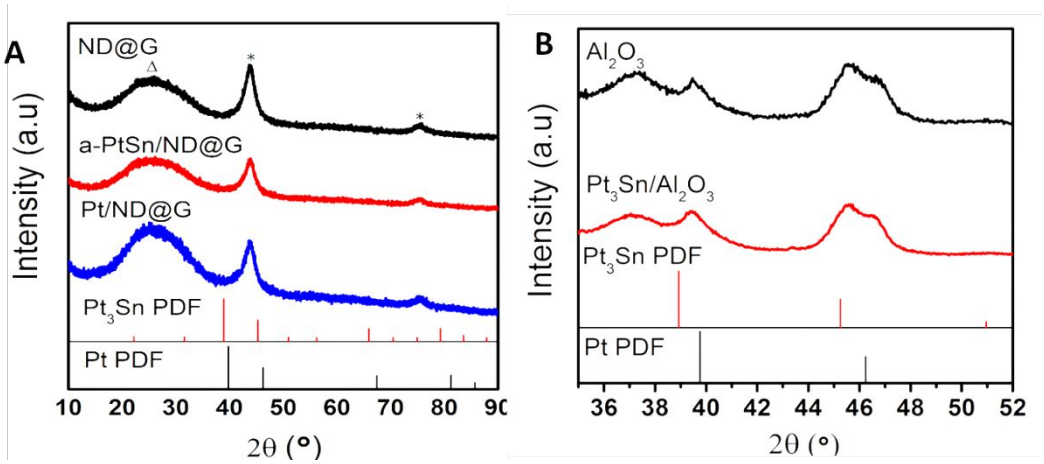

fig. S2. A） XRD patterns of a-PtSn/ND@G, Pt/ND@G catalyst, and pure ND@G support (∗, ND; Δ, graphene). B） XRD patterns of Pt_3Sn/ Al_2O_3 catalyst, and pure Al_2O_3 support.

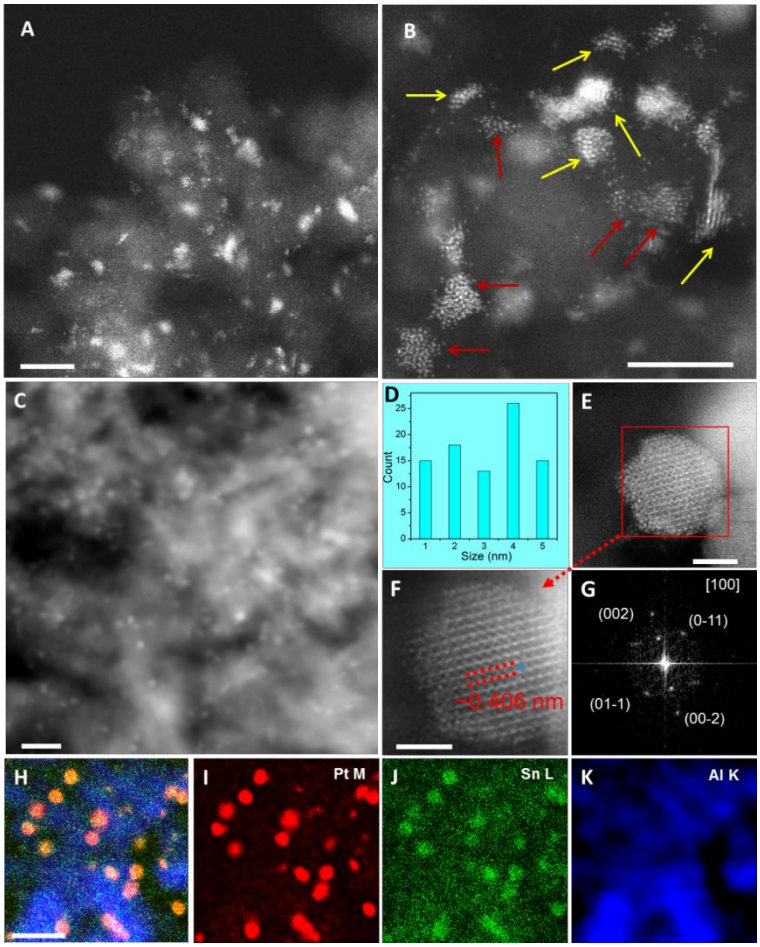

fig. S3. A) and B) HAADF-STEM images of the Pt/ND@G catalyst, scale bar, 5 nm, the red arrows and yellow arrows as marked in B) representing the atomically dispersed Pt clusters and Pt nanoparticles (with lattice structure) on ND@G support, respectively. C) HAADF-STEM images of the Pt_3Sn/Al_2O_3 catalyst, scale bar, 20 nm. D) The size distribution of the Pt_3Sn/Al_2O_3 catalyst and E-F) HAADF-STEM images of one randomly collected Pt_3Sn alloy nanoparticle, scale bar, 2 nm, and G) the corresponding area-indexed image with Fourier transform of one Pt_3Sn alloy nanoparticle. H-K) EDX mapping analysis of the Pt_3Sn/Al_2O_3 catalyst, scale bar, 20 nm.

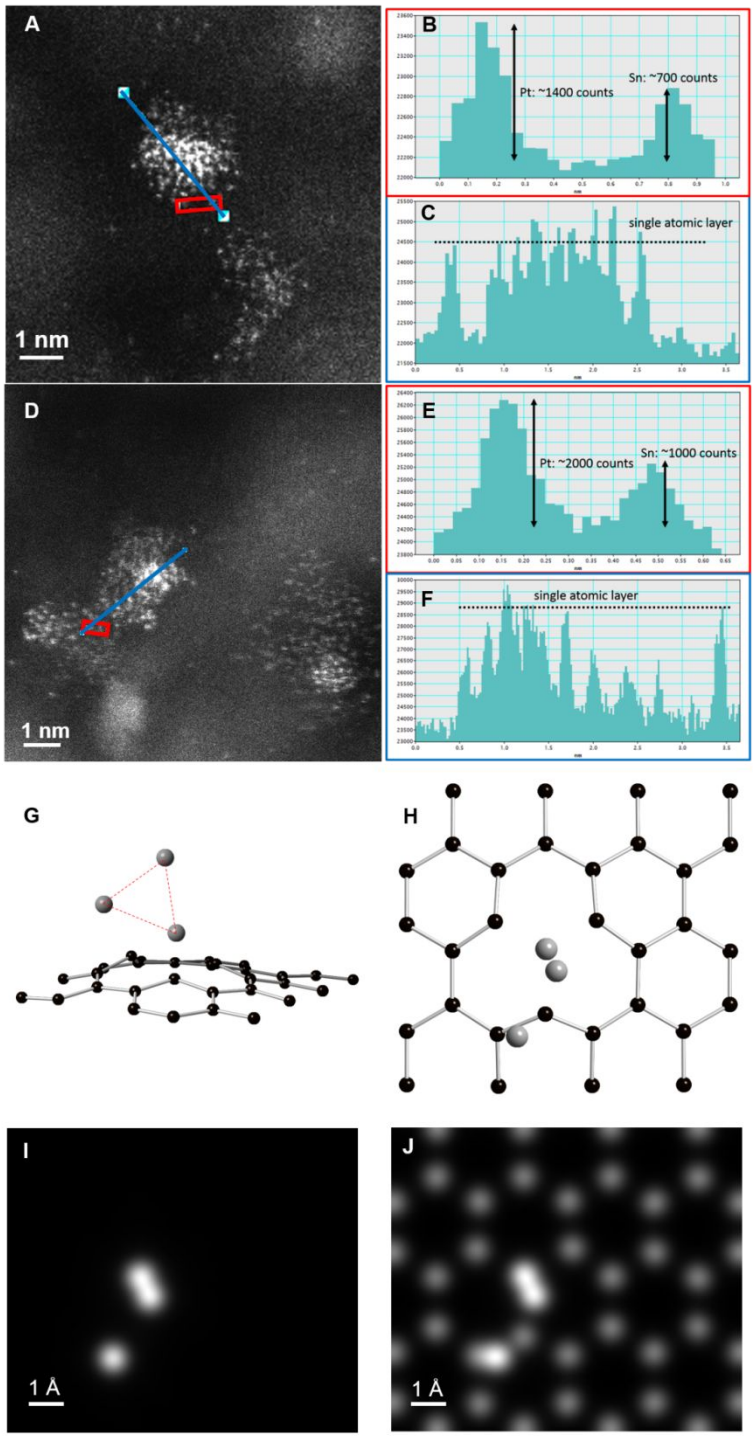

fig. S4. A) and **D**) HAADF-STEM image of a-PtSn/ND@G and the extracted line profiles **B-C**) and **E-F**) along red and blue directions in **A**) and **D**), respectively, demonstrating the pronounced intensity difference between Pt and Sn, as well as the single-atomic-layer thickness of a typical PtSn nanocluster, according to the Z-contrast imaging mechanism. **G-J)** HAADF-STEM image simulations. Atomic model **G**) showing a Pt_3 on defective graphene surface and its projection view **H**) along the

electron beam direction. **I**) Simulated image of the structure in **H**) using experimental parameters, where carbon atoms is invisible due to the low contrast. **J**) Simulated image of the same structure as **I**) but carbon atoms were artificially replaced by Sn atoms to demonstrate the distinguishable "Z-contrast" of Pt and Sn atoms.

It is clear from these results that the irregularly-shaped Pt particles are composed of random aggregates of ultra-small Pt clusters, and the Pt species are one atomic-layer-thick. Clearly, the planes of Pt_3 triangle and carbon support surface are not parallel with each other, which may explain the irregular atomic structures of Pt clusters under STEM due to the projection nature of TEM imaging mechanisms.

Table S1. Physicochemical parameters of different samples.

Sample	S_{BET} [m^2 g^{-1}]	Vt [cm^3 g^{-1}]	Average pore diameter [nm]	Dispersion of Pt[a] [%]	
				fresh	used
a-PtSn/ND@G	378	1.62	16.4	99.2	97.3
Pt_3Sn/Al_2O_3	134	0.83	23.0	74.7	65.3
Pt/ND@G	354	1.59	17.2	83.2	80.6

[a] Measured by H_2-O_2 titration method.

N_2 adsorption was employed to characterize the specific surface area and pore volume of the as-prepared samples (a-PtSn/ND@G and Pt_3Sn/Al_2O_3). Notably, the Al_2O_3 support has larger average pore diameter, while the BET and cumulative volume of pores of ND@G are larger than that of Al_2O_3 support.

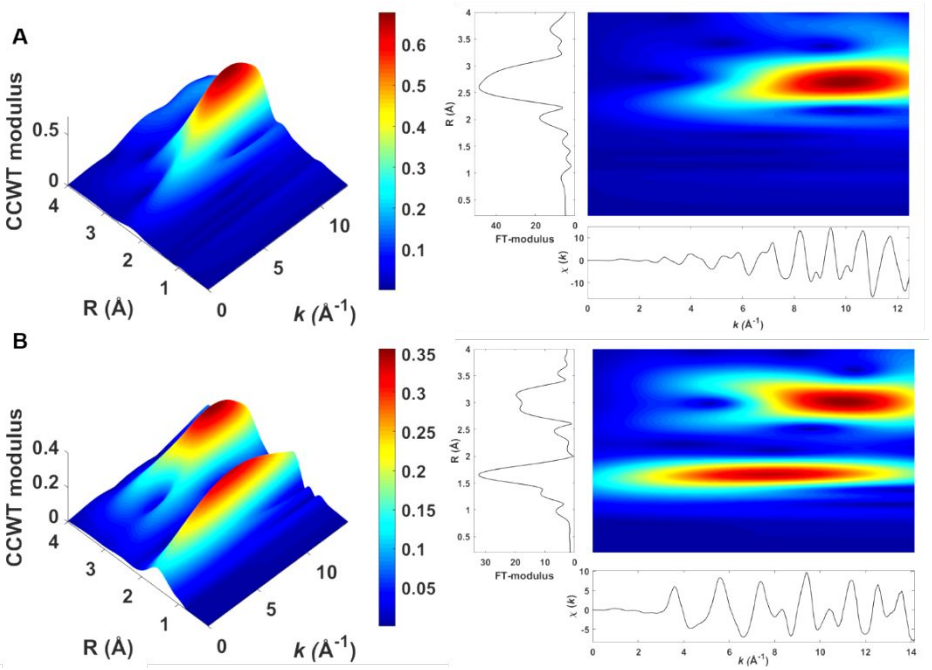

fig. S5. Wavelet transform (WT) analysis of **A**) Pt foil and **B**) PtO_2

Table S2. Pt L_3-edge and Sn K-edge EXAFS fitting results for a-PtSn/ND@G and Pt/ND@G.

Sample	Shell	C.N	R(Å)	$\Delta\sigma^2$(*10^{-3} Å^2)	ΔE_0 shift (eV)
a-PtSn/ND@G	Pt-Pt	1.8	2.75	9.3	7.6
	Pt-Sn	-	-	-	-
	Pt-C/O	2.2	2.02	3.1	7.6
	Sn-O	5.9	2.06	5.0	5.9
	Sn-Pt	-	-	-	-
	Sn-O-Sn_1	1.2	3.37	3.0	5.3
	Sn-O-Sn_2	4.8	3.89	3.0	5.3
Pt/ND@G	Pt-Pt	4.8	2.70	7.6	3.3
	Pt-C/O	2.1	2.03	2.1	3.3

EXAFS parameters characterizing a-PtSn/ND@G, Pt_3Sn/Al_2O_3 and Pt/ND@G. C.N., coordination number; R, distance between absorber and backscatter atoms; $\Delta\sigma^2$, disorder term; ΔE_0, inner potential correction. Error bounds characterizing the structural parameters obtained by EXAFS spectroscopy are estimated to be C.N., ± 20%; R, ± 0.02 Å; $\Delta\sigma^2$, ± 20%; ΔE_0, ± 20%.

For the a-PtSn/ND@G catalyst, the dominant scattering is Sn-O at a distance of 2.05 Å, with the average C.N. of 5.9. Meanwhile two Sn-O-Sn shells, with an average C.N. of 1.2 at a bond distance of 3.37 Å and 4.8 at a bond distance of 3.89 Å, are also resolved and denoted as Sn-O-Sn_1 and Sn-O-Sn_2. These results suggest that the Sn species are highly dispersed on ND@G support as tin oxide species, in good agreement with the X-ray absorption near edge structure (XANES) data as displayed in Figure S7.

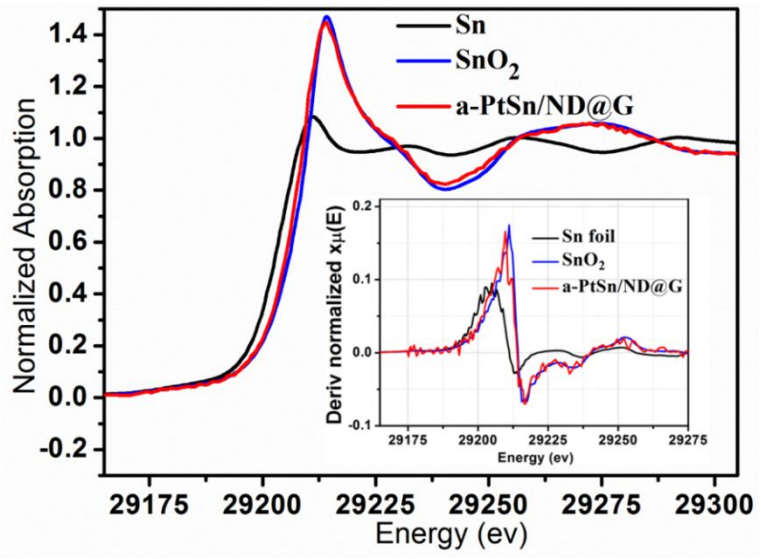

fig. S6. XANES data characterizing Sn foil, a-PtSn/ND@G, and SnO_2.

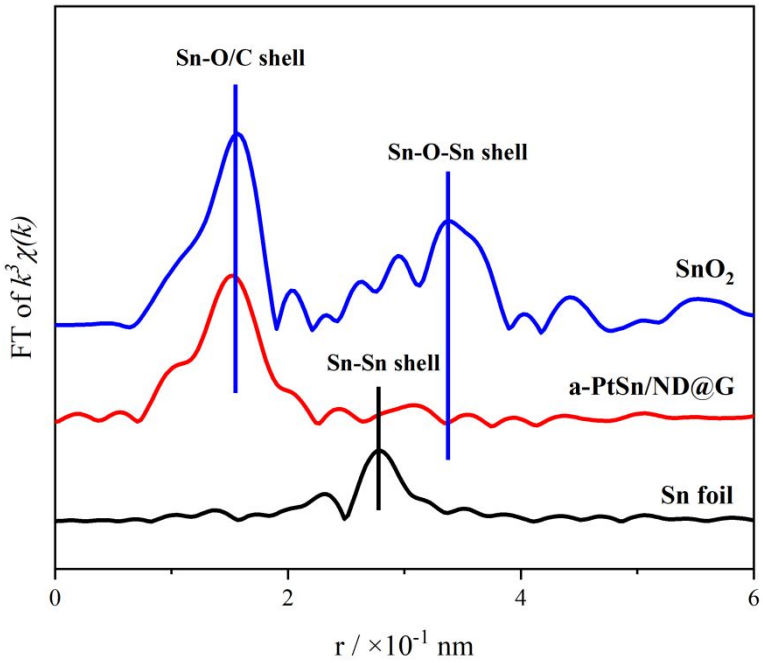

fig. S7. FT-EXAFS profiles of Sn K edge of a-PtSn/ND@G, Sn foil and SnO_2.

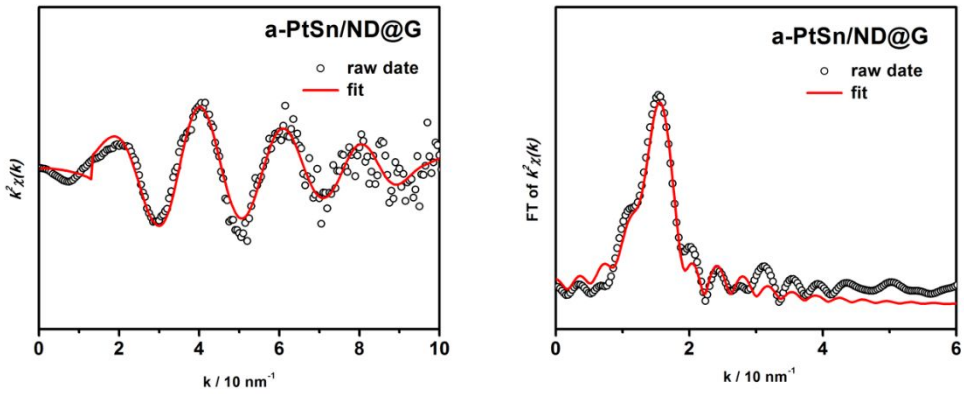

fig. S8. Sn K-edge EXAFS fitting results for a-PtSn/ND@G. Solid lines are fitting results, and dotted lines are EXAFS data.

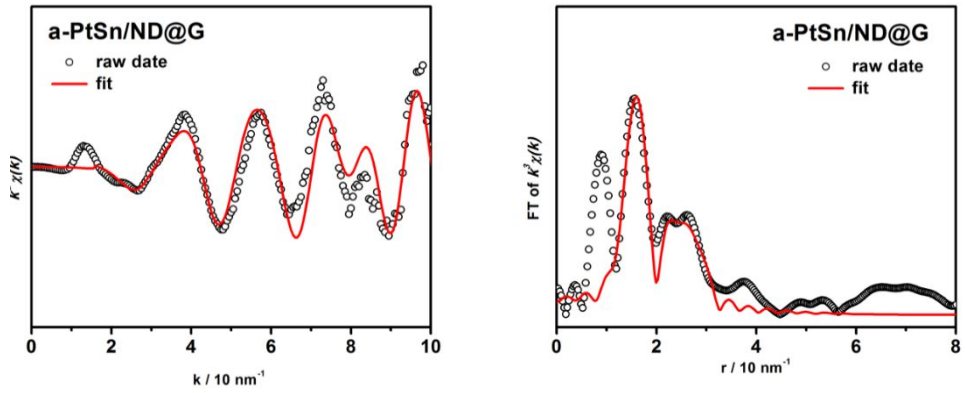

fig. S9. Pt L_3-edge EXAFS fitting results for a-PtSn/ND@G. Solid lines are fitting results, and dotted lines are EXAFS data.

Table S3. Activity performance of as-prepared catalysts for n-butane dehydrogenation reaction at 450 °C, GHSV=18000 mL/g_{cat}·h.

Catalyst	Conv. C_i/C_f (%)	Selectivity S_i/S_f (%)				Olefin Yield (Y_f) (%)	k_d[a] [h^{-1}]	τ[b] [h]
		1-butene	2-butene	1,3-butadiene	others			
a-PtSn/ND@G	40.9/35.6	23.4/23.7	70.1/71.1	4.7/3.9	1.8/1.4	35.2	0.0124	80.6
Pt_3Sn/Al_2O_3	13.6/6.2	22.1/23.8	65.6/68.7	4.4/4.8	7.9/2.7	6.0	0.0495	20.2
Pt/ND@G	24.4/13.4	22.0/23.3	65.6/68.8	4.0/4.4	8.4/3.5	13.5	0.0510	24.1

i: initial catalytic valueafter reaction 30min.

f: final catalytic value after reaction 18h.

[a]: k_d, deactivation rate constant, calculated from $k_d = \{\ln[(1-C_f)/C_f] - \ln[(1-C_i)/C_i]\}/t$.

[b]: τ represents the catalyst life, which is the reciprocal of the deactivation rate constants ($\tau = 1/k_d$), and means time required for rates to decrease by e^{-1}.

The DDH stability was evaluated by a first–order deactivation as shown in **Table S4**. The a-PtSn/ND@G catalyst displays a lower deactivation rate (0.0124 h^{-1}) and longer catalyst life time (80.6 h), illustrating its higher activity and stability in comparison with that of the typical Pt_3Sn/Al_2O_3 and Pt/ND@G catalyst.

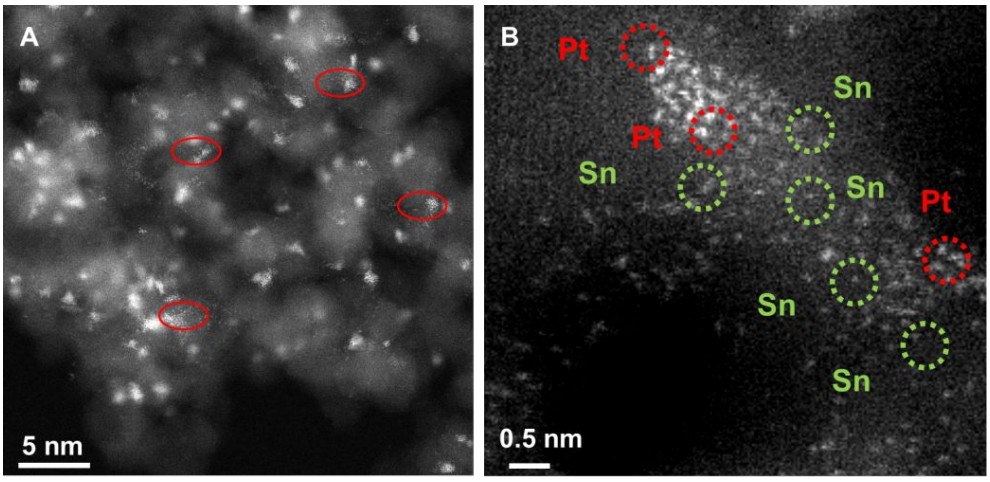

fig. S10. HAADF-STEM characterization of the used a-PtSn/ND@G catalyst showing the homogeneous dispersion of Pt clusters **A**) and atomic dispersion of Pt cluster and Sn species on ND@G marked out by red (Pt) and green (Sn) circles **B**).

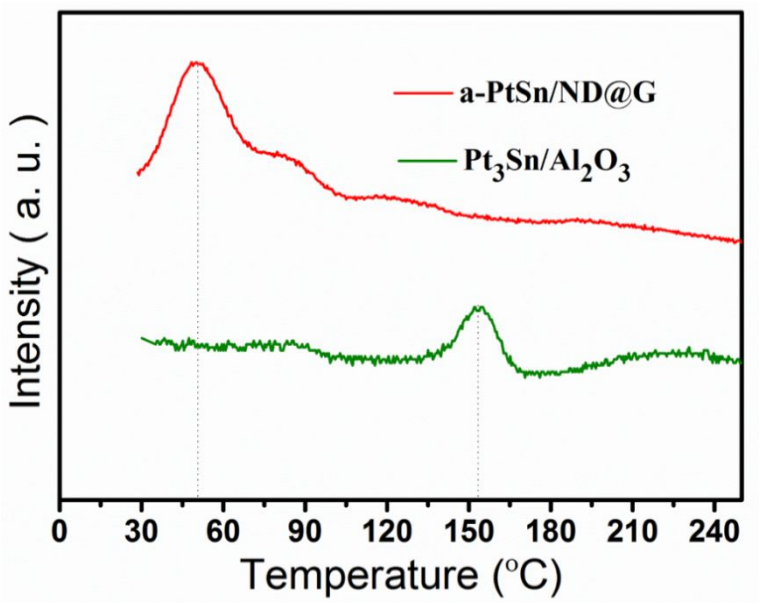

fig. S11. *n*-C_4H_8-TPD profiles of a-PtSn/ND@G and Pt_3Sn/Al_2O_3 catalysts.

Table S4. Summary of the reaction performance of various Pt-based catalysts for the direct dehydrogenation of n-Butane.

Catalyst	T (°C)	GHSV ($mL/g_{cat}\cdot h$)	Feed	Conversion (%)	Selectivity (%)	Ref.
0.3wt%Pt-Sn/$MgAl_2O_3$	530	5400	nC_4/H_2=1.25 N_2=44.5	32-28 (10 min-2 h)	97.0	3
0.3wt%Pt-Sn/Y-Al_2O_3	530	5400	nC_4/H_2=1.25 He=44.5	30-28 (10 min-2 h)	94.4	4
0.89wt%Pt-In/Mg(Al)(In)O	530	960000	nC_4/H_2=2.5 He=54.5	13-7.5 (10 min-2 h)	95.0	5
Pt/Sn/Zn/γ-Al_2O_3	550	600	nC_4/N_2=1:1	76.0-59.1 (1 h-6 h)	84.8	6
a-PtSn/ND@G	450	18000	$nC_4/H_2/N_2$=1:1:48	40.9-35.7 (30 min-18 h)	98.7	This work

Table S5. Energies (DFT calculation) of possible Pt_3O_1-graphene structures (Pt: blue; O: red; C: grey).

Labels	Structures	Energies(eV)	Labels	Structures	Energies(eV)
a)	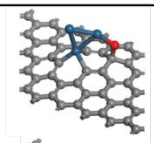	-465.62	f)	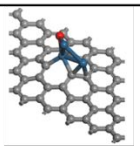	-466.28
b)	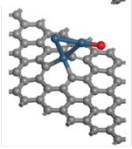	-466.38	g)	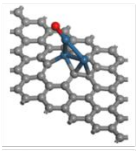	-466.02
c)	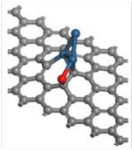	-464.94	h)	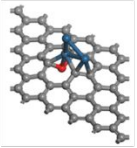	-465.70
d)	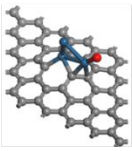	-465.50	i)	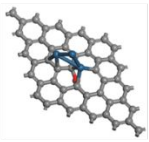	-465.72
e)	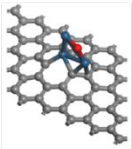	-466.30			

Table S6. Energies (DFT calculations) of possible Pt_3O_2-graphene structures (Pt: blue; O: red; C: grey).

Labels	Structures	Energies(eV)	Labels	Structures	Energies(eV)
(a)	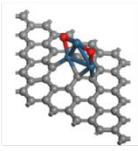	-473.21	(g)	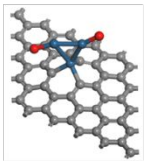	-472.31
(b)	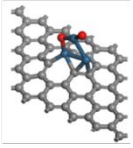	-473.0	(h)	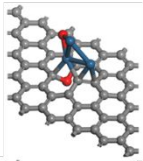	-471.42
(c)	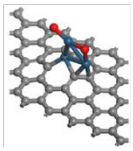	-473.01	(i)	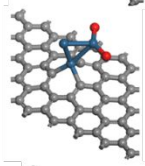	-471.99
(d)	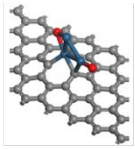	-472.00	(j)	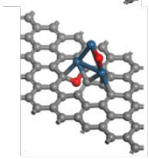	-471.67
(e)	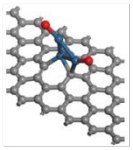	-472.05	(k)	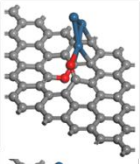	-473.19
(f)	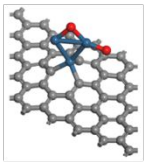	-472.41	(l)	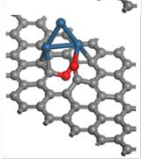	-472.20

Table S7. Energies (DFT calculations) of possible Pt_3O_3-graphene structures (Pt: blue; O: red; C: grey).

Labels	Structures	Energies(eV)	Labels	Structures	Energies(eV)
a)	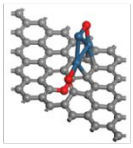	-479.03	e)	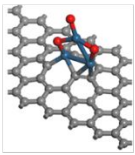	-478.72
b)	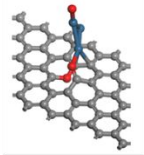	-479.19	f)	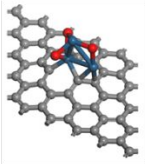	-478.07
c)	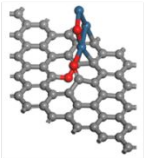	-479.45	g)	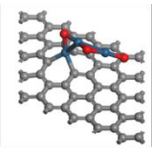	-479.77
d)	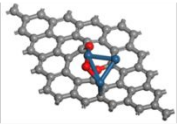	-478.04	h)	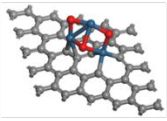	477.35

We calculated the change of Gibbs free energies from the most stable Pt_3O_x-graphene to Pt_3-graphene under reaction condition (T = 450 °C, P (H_2) = 0.02Bar.):

Pt_3O_3-graphene + $3H_2(g)$ = Pt_3-graphene + $3H_2O(g)$ (1) ΔG = -2.57eV

Pt_3O_2-graphene + $2H_2(g)$ = Pt_3-graphene + $2H_2O(g)$ (2) ΔG = -1.79 eV

Pt_3O_1-graphene + $H_2(g)$ = Pt_3-Gr + $H_2O(g)$ (3) ΔG = -1.16 eV

ΔG of the reaction (1) - (3) are -2.57, -1.79 and -1.16 eV, indicating that Pt_3O_3-graphene, Pt_3O_2-graphene and Pt_3O_1-graphene will be reduced to Pt_3-graphene under the reaction condition (diluted H_2 at 450 °C). Therefore, Pt_3-Gr model is chosen to present the working catalyst to investigate reaction activities and product selectivity.

The Gibbs free energy of H_2 and H_2O gas species (T = 450 °C, P (H_2) = 0.02 P^o, P (H_2O) = P^o), is calculated by:

$$G\ (g, T/K, P) = E_{DFT} + E_{ZPE} + nRT - TS + RT\ln(P/P^0) \quad (4)$$

The Gibbs free energy of Pt_3O_3-graphene, Pt_3O_2-graphene and Pt_3O_1-graphene, including the O species zero-point energy, is calculated by:

$$G\ (\text{Adsorbed species}, T/K, P) = E_{DFT} + E_{ZPE} \quad (5)$$

The Gibbs free energy of Pt_3-graphene is calculated by:

$$G\ (T/K, P) = E_{DFT} \quad (6)$$

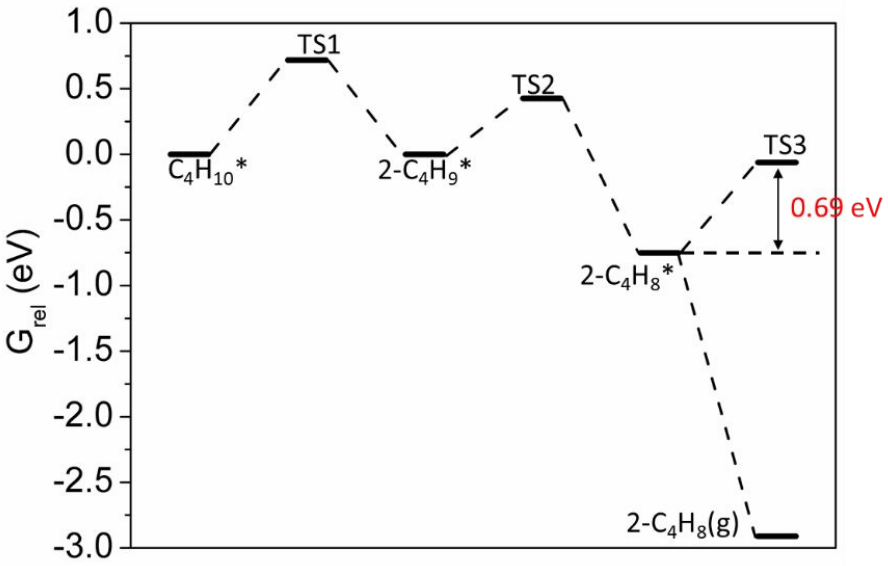

fig. S12. Relative Gibbs free energy profile (T = 450 °C) of butane dehydrogenation on the Pt_3Sn-(111) surface.

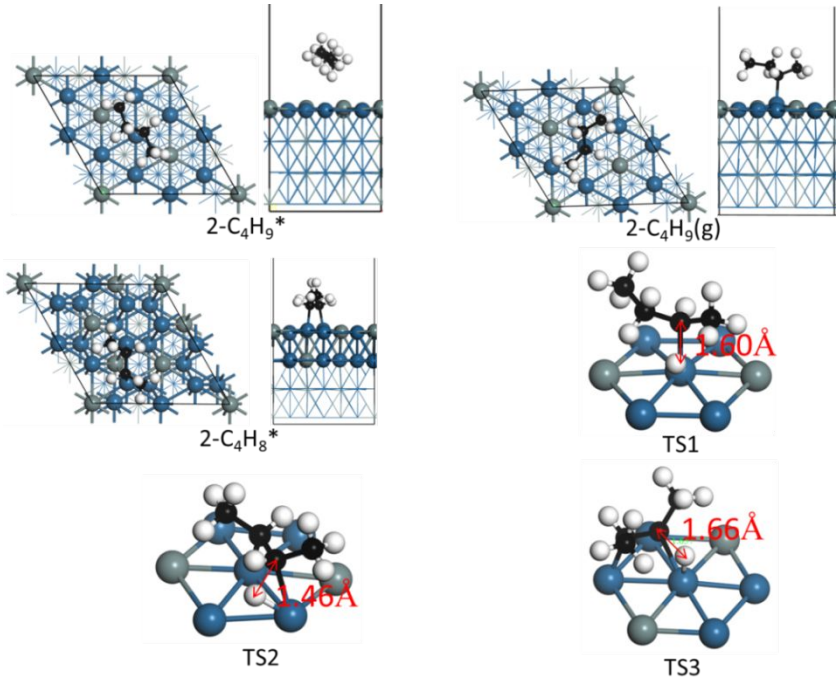

fig. S13. The structures for intermediates and transition states from C_4H_{10} to 2-C_4H_8 on Pt_3Sn-(111). Black: C, White: H, Blue: Pt, Gray: Sn.

Table S8. Step by step barrier (ΔG_a, eV) and enthalpy energy change (ΔH_r, eV) for n-butane dehydrogenation to 2-butene on Pt_3-graphene and Pt_3Sn-(111) surface.

	Pt_3-graphene		Pt_3Sn-(111)	
Reactions	ΔH_r (eV)	ΔG_a (eV)	ΔH_r (eV)	ΔG_a (eV)
$C_4H_{10}(g) \rightarrow C_4H_{10}*$	-0.27	2.87	-0.11	3.09
$C_4H_{10}* \rightarrow 2\text{-}C_4H_9* + H*$	-0.53	0.11	0.00	0.72
$2\text{-}C_4H_9* \rightarrow 2\text{-}C_4H_8* + H*$	-0.63	0.01	-0.75	0.43
$2\text{-}C_4H_8* \rightarrow 2\text{-}C_4H_7* + H*$	--	1.34	--	0.69
$2\text{-}C_4H_8* \rightarrow 2\text{-}C_4H_8(g)$	1.22	--	0.66	--

Table S9. The energy change of Pt3@Gr structure with the increased k-points mesh.

k-points mesh	E, eV
1 x 1 x 1	-460.12
2 x 2 x 1	-460.75
3 x 3 x 1	-460.69
4 x 4 x 1	-460.69
5 x 5 x 1	-460.69

Table S10. The reaction energies and activation energies of butane to 2-butene on Pt3@Gr using PBE, HSE06 functional, respectively**.**

	PBE(3 x 3 x 1)	HSE06(3 x 3 x 1)
R1: $C_4H_{10}(g) \rightarrow C_4H_{10}*$		
ΔE	-0.27	-0.26
R2: $C_4H_{10}* \rightarrow 2\text{-}C_4H_9*$		
ΔE	-0.53	-0.59
Ea	0.11	0.14
R3: $2\text{-}C_4H_9* \rightarrow 2\text{-}C_4H_8*$		
ΔE	-0.63	-0.71
Ea	0.01	0.02
R4: $2\text{-}C_4H_8* \rightarrow 2\text{-}C_4H_8(g)$		
ΔE	1.22	1.36
R5: $2\text{-}C_4H_8* \rightarrow 2\text{-}C_4H_7*$		
Ea	1.34	1.46

a. Brackets indicate k-points mesh.

Supporting References

(1) M. Ozawa, M. Inaguma, M. Takahashi, F. Kataoka, A. Krüger, E. Ōsawa, Preparation and Behavior of Brownish, Clear Nanodiamond Colloids. *Adv. Mater.* **19**, 1201-1206 (2007).

(2) J. Liu, Y. Yue, H. Liu, Z. Da, C. Liu, A. Ma, J. Rong, D. Su, X. Bao, H. Zheng, Origin of the Robust Catalytic Performance of Nanodiamond–Graphene-Supported Pt Nanoparticles Used in the Propane Dehydrogenation Reaction *ACS Catal.* **7**, 3349-3355 (2017).

(3) S. Bocanegra, O. Scelza, S. de Miguel, Effect of the Synthesis Method of $MgAl_2O_4$ and of Sn and Pb Addition to Platinum Catalysts on the Behavior in n-Butane Dehydrogenation. *Ind. Eng. Chem. Res.* **49**, 4044-4054 (2010).

(4) A. D. Ballarini, P. Zgolicz, I. M. J. Vilella, S. R. de Miguel, A. A. Castro, O. A. Scelza, A. n-Butane dehydrogenation on Pt, PtSn and PtGe supported on γ-Al_2O_3 deposited on spheres of α-Al_2O_3 by washcoating. *Appl. Catal. A-Gen.* **381**, 83-91 (2010).

(5) J. Wu, Z. Peng, P. Sun, A. T. Bell, n-Butane dehydrogenation over Pt/Mg(In)(Al)O. *Appl. Catal. A-Gen.* **470**, 208-214 (2014).

(6) H. Seo, J. K. Lee, U. G. Hong, G. Park, Y. Yoo, J. Lee, H. Chang, I. K. Song, Direct dehydrogenation of n-butane over Pt/Sn/M/γ-Al_2O_3 catalysts: Effect of third metal (M) addition. *Catal. Commun*. **47**, 22-27 (2014).